

Multi- \bar{K} nuclei and kaon condensation

D. Gazda,^{1,*} E. Friedman,^{2,†} A. Gal,^{2,‡} and J. Mareš^{1,§}

¹*Nuclear Physics Institute, 25068 Řež, Czech Republic*

²*Racah Institute of Physics, The Hebrew University, Jerusalem 91904, Israel*

(Dated: August 26, 2021)

Abstract

We extend previous relativistic mean-field (RMF) calculations of multi- \bar{K} nuclei, using vector boson fields with SU(3) PPV coupling constants and scalar boson fields constrained phenomenologically. For a given core nucleus, the resulting \bar{K} separation energy $B_{\bar{K}}$, as well as the associated nuclear and \bar{K} -meson densities, saturate with the number κ of \bar{K} mesons for $\kappa > \kappa_{\text{sat}} \sim 10$. Saturation appears robust against a wide range of variations, including the RMF nuclear model used and the type of boson fields mediating the strong interactions. Because $B_{\bar{K}}$ generally does not exceed 200 MeV, it is argued that multi- \bar{K} nuclei do not compete with multihyperonic nuclei in providing the ground state of strange hadronic configurations, and that kaon condensation is unlikely to occur in strong-interaction self-bound strange hadronic matter. Last, we explore possibly self-bound strange systems made of neutrons and \bar{K}^0 mesons, or protons and K^- mesons, and study their properties.

PACS numbers: 13.75.Jz; 21.65.Jk; 21.85.+d; 26.60.-c

Keywords: \bar{K} -nuclear RMF calculations; \bar{K} -nuclear bound states; kaon condensation; neutron stars

*Electronic address: gazda@ujf.cas.cz

†Electronic address: elifried@vms.huji.ac.il

‡Electronic address: avragal@vms.huji.ac.il

§Electronic address: mares@ujf.cas.cz

I. INTRODUCTION AND OVERVIEW

Kaon condensation in dense matter was proposed over 20 years ago by Kaplan and Nelson [1, 2]. It is necessary to distinguish in this context between K mesons and \bar{K} mesons which interact quite differently with matter. The empirical evidence from K^- atoms is that the \bar{K} -nuclear interaction is strongly attractive, and absorptive as well, with typical values of 150–200 MeV attraction at nuclear-matter density ρ_0 , as reviewed recently by Friedman and Gal [3]. A strong nuclear attraction of somewhat less than 100 MeV at ρ_0 for K^- mesons, compared to a weak repulsion of order 25 MeV for K^+ mesons, follows from observations of enhanced near-threshold production of K^- mesons in proton-nucleus collisions at GSI [4]. This weakly repulsive nature of the K^+ -nuclear interactions was quantified a long time ago, starting with Dover and Moffa [5], and is also reviewed in Ref. [3]. Given the distinction between the nuclear interactions of K mesons and \bar{K} mesons, the term *kaon condensation* is used loosely here and elsewhere to mean \bar{K} condensation.

Neutron stars, with a density range extending over several times ρ_0 , offer the most natural dense systems where kaon condensation could be realized; see Refs. [6, 7, 8, 9, 10, 11] for comprehensive reviews of past work. We note that in *Heaven*, for neutron stars, weak-interaction time scales of order 10^{-8} s and longer are operative, enabling strangeness-changing processes such as $e^- \rightarrow K^- + \nu_e$ to transform high-pressure dense electrons to K^- mesons once the effective mass of K^- mesons drops down below approximately 200 MeV. Under some optimal conditions, recalling that \bar{K} mesons undergo attraction of order 100 MeV per density unit of ρ_0 [12], kaon condensation could occur at densities about $3\rho_0$, depending on the way hyperons enter the constituency of neutron stars as first recognised by Ellis, Knorren and Prakash [13]. However, on *Earth* under laboratory conditions, strong-interaction time scales of order 10^{-23} s are operative; processes of equilibration and hadronization subsequent to dense-matter formation in heavy-ion collisions occur over much shorter times than those controlling the composition of neutron stars. If antikaons bind strongly to nuclei, according to a scenario spelled out recently by Yamazaki *et al.* [14], then \bar{K} mesons might provide the relevant physical degrees of freedom for self-bound strange hadronic matter that would then be realized as multi- \bar{K} nuclei. It requires that the \bar{K} separation energy $B_{\bar{K}}$ beyond some threshold value of strangeness exceeds $m_K c^2 + \mu_N - m_\Lambda c^2 \gtrsim 320$ MeV, where μ_N is the nucleon chemical potential, thus allowing for the conversion $\Lambda \rightarrow \bar{K} + N$ in matter.

For this strong binding, Λ and Ξ hyperons would no longer combine macroscopically with nucleons to compose the more conventional kaon-free form of strange hadronic matter [15]. \bar{K} mesons will then condense macroscopically. However, the nuclear densities encountered in these strange hadronic nuclei are somewhat less than the typical $3\rho_0$ threshold required to lower sufficiently the \bar{K} energy in matter to reach condensation. Yet, precursor phenomena to kaon condensation in nuclear matter could occur at lower densities as soon as $B_{\bar{K}}$ exceeds the combination $m_{\bar{K}}c^2 + \mu_N - m_{\Sigma}c^2 \gtrsim 240$ MeV. In this case, the only mechanism underlying the widths of multi- \bar{K} states is the fairly weak conversion $\bar{K}NN \rightarrow \Lambda N$.

Recently we have reported on preliminary calculations of multi- \bar{K} nuclear configurations [16] using the relativistic mean-field (RMF) methodology, constrained by \bar{K} -nucleus phenomenology. It was found that the nuclear and \bar{K} densities behave regularly on increasing the number of antikaons embedded in the nuclear medium, without any indication for abrupt or substantial increase, and that the \bar{K} separation energy saturates. Roughly speaking, the heavier the nucleus is, the more antikaons it takes to saturate the separation energies, but even for ^{208}Pb the number required does not exceed approximately 10. Because the calculated \bar{K} separation energies $B_{\bar{K}}$ do not generally exceed 200 MeV, for input binding in the accepted “deep-binding” range $B_{\bar{K}} \sim 100 - 150$ MeV for a single \bar{K} meson [17, 18, 19], it was deemed unlikely that kaon condensation occurs in nuclear matter. This leaves antikaons in multi- \bar{K} nuclei comfortably above the range of energies appropriate to (hyperonic) strange hadronic matter [15]. In the present article we discuss the full scope of these calculations demonstrating the robustness of this saturation property. In particular we study the sensitivity of the results to the nuclear equation of state used, through the nonlinear RMF version employed, and the role of “hidden strangeness” isoscalar meson fields beyond the standard isoscalar, scalar (σ), and vector (ω) meson fields. Although both σ - and ω -meson fields mediate attraction between \bar{K} mesons and nucleons, they play different roles for the interactions within \bar{K} mesons, similarly to the pattern well known for nucleons. The σ meson induces attraction, whereas the ω meson induces repulsion. If the \bar{K} -meson couplings were exclusively limited to scalar-meson fields, the resulting \bar{K} -meson separation energies would not have saturated. However, chiral model studies of $\bar{K}N$ low-energy phenomenology give a clear evidence in favor of the lowest-order Tomozawa-Weinberg *vector* interaction, which in terms of meson exchanges is equivalent to vector-meson exchanges with purely F-type SU(3) pseudoscalar-pseudoscalar-vector (PPV) vertices [19]. Our philosophy in this work is to use

these vector-meson fields coupling constants as they are, augmenting the \bar{K} -nucleus vector interaction by additional *scalar* couplings such that $B_{\bar{K}} \sim 100 - 150$ MeV holds for single- \bar{K} nuclei. We find no precursor behavior to kaon condensation for \bar{K} mesons in self-bound nuclear matter.

We also explore in this work exotic strange self-bound configurations where \bar{K} mesons are bound to either neutrons or protons. The simple example of a quasibound K^-pp system (and thus also its charge-symmetric partner \bar{K}^0nn) recently calculated solving Faddeev coupled-channel equations [20, 21, 22], clearly demonstrates that \bar{K} mesons can bind together nuclear clusters that are otherwise unbound. The point here is that the underlying K^-p and \bar{K}^0n interactions (each with equally mixed $I = 0$ and $I = 1$ components) provide considerably more attraction than the purely $I = 1$ K^-n and \bar{K}^0p interactions. The RMF calculations reported here start with eight neutrons, showing that a finite number of neutrons can be made self bound by adding together a few \bar{K}^0 mesons, with \bar{K} separation energies of order $B_{\bar{K}} \sim 50 - 100$ MeV. We study the role of the isovector ρ meson in stabilizing these exotic configurations, owing to its role in distinguishing between the underlying $I = 0$ and $I = 1$ $\bar{K}N$ interactions. We find that the emergent stable neutron configurations are more tightly bound than in the corresponding ordinary nuclei with $N \approx Z$ along the stability valley, and the neutron single-particle spectra display substantial rearrangement. However, these exotic configurations are found to be unstable against charge-exchange $\bar{K}^0 + n \rightarrow K^- + p$ reactions.

In Sec. II we briefly outline the RMF methodology and discuss the \bar{K} coupling constants to the meson fields used in the present calculations. Results are shown and discussed in Sec. III for \bar{K} separation energies and density distributions, also displaying the dependence on the type of nonlinear RMF model used and the contribution of specific meson fields to the energy systematics and particularly to maintaining saturation in a robust way. A separate subsection is devoted to the study of exotic multi- \bar{K} “nuclei” with neutrons only. Again, binding energies and densities are discussed, plus rearrangement features of the neutrons in the \bar{K} -extended mean field. We conclude with a brief summary in Sec. IV.

II. METHODOLOGY

A. RMF equations of motion

Bound nuclear systems of nucleons and several \bar{K} mesons are treated in this work within the RMF framework, where the interactions among hadrons are mediated by the exchange of scalar- and vector-meson fields. The model Lagrangian consists of a standard nuclear part \mathcal{L}_N and the Lagrangian density \mathcal{L}_K describing the kaonic sector:

$$\mathcal{L}_K = (\mathcal{D}_\mu K)^\dagger (\mathcal{D}^\mu K) - m_K^2 K^\dagger K + g_{\sigma K} m_K K^\dagger K \sigma + g_{\sigma^* K} m_K K^\dagger K \sigma^*. \quad (1)$$

Here,

$$\mathcal{D}_\mu \equiv \partial_\mu + i g_{\omega K} \omega_\mu + i g_{\rho K} \vec{\tau} \cdot \vec{\rho}_\mu + i g_{\phi K} \phi_\mu + i e \frac{1}{2} (1 + \tau_3) A_\mu, \quad (2)$$

and K (K^\dagger) denotes the kaon (antikaon) doublet. To be specific, we discuss K^- -nuclear systems. Similar expressions hold for \bar{K}^0 mesons. In addition to a scalar-meson field σ and to vector-meson fields ω and ρ normally used in purely nuclear RMF calculations, we also considered meson fields that couple exclusively to strangeness degrees of freedom, a scalar σ^* , and a vector ϕ . Standard techniques yield a coupled system of equations of motion for nucleons and all meson mean fields involved; we refer the reader to our earlier work [16] for details. Here it suffices to recall that the presence of \bar{K} meson(s) induces additional source terms in the Klein-Gordon (KG) equations for the meson (mean) fields. In the case of K^- mesons, the source terms contain the K^- density

$$\rho_{K^-} = 2(E_{K^-} + g_{\omega K} \omega_0 + g_{\rho K} \rho_0 + g_{\phi K} \phi_0 + e A_0) K^- K^+, \quad \int d^3x \rho_{K^-} = \kappa, \quad (3)$$

where $E_{K^-} = i \partial_t K^-$. Hence, the \bar{K} mesons modify the scalar and vector potentials that enter the Dirac equation for nucleons, thus leading to rearrangement of the nuclear core. The polarized nucleons, in turn, modify the \bar{K} -nucleus interaction. This calls for a self-consistent procedure for solving the equations of motion.

In our model, the KG equation of motion for the K^- meson acquires the form

$$[-\nabla^2 - E_{K^-}^2 + m_K^2 + \text{Re} \Pi_{K^-}] K^- = 0, \quad (4)$$

with the K^- self-energy given by

$$\begin{aligned} \text{Re} \Pi_{K^-} = & - (g_{\sigma K} m_K \sigma_0 + g_{\sigma^* K} m_K \sigma_0^*) - 2E_{K^-} (g_{\omega K} \omega_0 + g_{\rho K} \rho_0 + g_{\phi K} \phi_0 + e A_0) \\ & - (g_{\omega K} \omega_0 + g_{\rho K} \rho_0 + g_{\phi K} \phi_0 + e A_0)^2. \end{aligned} \quad (5)$$

Of the three terms on the right-hand side (rhs) of Eq. (5), the first one is a scalar-meson contribution, whereas the other two terms are vector-meson contributions. The scalar contribution is sometimes lumped together with the kaon mass m_K to form a density-dependent effective kaon mass m_K^* via

$$m_K^{*2} = m_K^2 - g_{\sigma K} m_K \sigma_0 - g_{\sigma^* K} m_K \sigma_0^*. \quad (6)$$

Finally, to account for K^- absorption in the nuclear medium, the self-energy $\Pi_{K^-} = 2E_{K^-} V_{\text{RMF}}^{K^-}$ in Eq. (4) was made complex by adding $\text{Im} \Pi_{K^-}$ and the real energy E_{K^-} was replaced by $E_{K^-} - i\Gamma_{K^-}/2$. The imaginary part of the self-energy, $\text{Im} \Pi_{K^-}$, was taken from optical model phenomenology, with a strength fitted to K^- atomic data [23] and with energy dependence that follows the reduced phase space for the decaying initial state. We assumed two-body final-state kinematics for the decay products in the absorption channels $\bar{K}N \rightarrow \pi Y$ ($Y = \Sigma, \Lambda$) (80%) and $\bar{K}NN \rightarrow YN$ (20%) with branching ratios indicated in parentheses [17, 18].

The set of coupled equations containing the Dirac equation for nucleons, the KG equations for the meson mean fields and for antikaons was solved fully self-consistently using an iterative procedure. This appeared crucial for the proper evaluation of the dynamical effects in nuclei with κ ($\kappa = 1, 2, 3, \dots$) \bar{K} mesons. The \bar{K} separation energy

$$B_{\bar{K}} = B[A, Z, \kappa \bar{K}] - B[A, Z, (\kappa - 1) \bar{K}], \quad (7)$$

where $B(A, Z, \kappa \bar{K})$ is the binding energy of the $\kappa \bar{K}$ -nuclear system, contains mean-field contributions due to rearrangement of the nuclear core.

B. Choice of parameters

For the nucleonic Lagrangian density \mathcal{L}_N we used the RMF parameter sets NL-SH [24] and NL-TM1(2) [25] which have been successfully used in numerous calculations of various nuclear systems. For the (anti-)kaon coupling constants to the vector-meson fields, we used a purely F-type SU(3) symmetry, $\alpha_V \equiv F/(F + D) = 1$:

$$2g_{\omega K} = \sqrt{2} g_{\phi K} = 2 g_{\rho K} = g_{\rho\pi} = 6.04, \quad (8)$$

where the value of $g_{\rho\pi}$ is due to the $\rho \rightarrow 2\pi$ decay width. As mentioned in Sec. I, this choice corresponds to the underlying Tomozawa-Weinberg lowest-order term in chiral perturbation

theory [19]. The value of $g_{\omega K}^{\text{SU}(3)} = 3.02$ adopted here is considerably lower than the quark-model (QM) value applied to NL-SH, $g_{\omega K} = \frac{1}{3}g_{\omega N}^{\text{NL-SH}} = 4.32$, which was used in our previous work [16], and we consider it to be the minimal value suggested by theory. The \bar{K} RMF *vector* potential at threshold in nuclear matter is then given, in the static approximation, by using the last two terms on the rhs of Eq. (5):

$$V_{\text{RMF-vector}}^{K^-} = -\frac{g_{\omega K}^{\text{SU}(3)} g_{\omega N}^{\text{NL-SH}} \rho_0}{m_\omega^2} - \frac{1}{2m_K} \left(\frac{g_{\omega K}^{\text{SU}(3)} g_{\omega N}^{\text{NL-SH}} \rho_0}{m_\omega^2} \right)^2 = -76.7 \text{ MeV}, \quad (9)$$

with $m_\omega = 783 \text{ MeV}$ and $\rho_0^{\text{NL-SH}} = 0.146 \text{ fm}^{-3}$. We point out that the value $g_{\omega N}^{\text{NL-SH}} = 12.95$ is not far away from the value $g_{\omega N}^{\text{ESC04}} = 11.06$ from the latest NN -potential fit by the Nijmegen group [26]. This latter value was obtained in that NN analysis after allowing for part of the isoscalar vector-meson field strength to result from a combined ρ - π exchange. We also studied the role of isovector \bar{K} nucleus interactions by comparing the results of using the present SU(3) choice $g_{\rho K}^{\text{SU}(3)} = 3.02$ with results applying a QM *universal* isospin coupling to NL-SH: $g_{\rho K} = g_{\rho N}^{\text{NL-SH}} = 4.38$. This value is substantially higher than the Nijmegen potential fit value $g_{\rho N}^{\text{ESC04}} = 2.77$, apparently to compensate for disregarding the almost four times higher value of the tensor coupling constant $f_{\rho N}^{\text{ESC04}}$.

SU(3) symmetry is not much of help in fixing the (anti-)kaon coupling to the scalar-meson field σ , simply because the microscopic origin of the σ field and its various couplings are not unambiguous. It has been shown recently that interpreting the σ field in terms of a $(J^\pi, I) = (0^+, 0)$ resonance in the $\pi\pi$ - $K\bar{K}$ coupled-channel system leads to a vanishing $\bar{K}N$ forward-scattering amplitude at threshold, thus suggesting a vanishing contribution to the corresponding \bar{K} -nucleus optical potential [27]. However, even for the empirically large value of $g_{\sigma N}$ obtained in the NN case ($g_{\sigma N}^{\text{ESC04}} = 10.17$) and also within the RMF description of nuclei, there is no consensus on its microscopic origin, except that QCD sum-rules do produce strong scalar condensates. Modern NN potentials using chiral perturbation theory guidelines obtain a rather strong isoscalar-scalar two-pion exchange contribution involving excitation of $\Delta(1232)$ in intermediate states [28]. A similar two-pion exchange contribution for $\bar{K}N$, involving the excitation of $K^*(892)$, cannot be excluded at present. In the absence of QCD sum-rule determinations of $g_{\sigma K}$, one relies for an order of magnitude estimate on simplified models such as the QM, giving rise to $g_{\sigma K}^{\text{QM}} = \frac{1}{3}g_{\sigma N}$, which for the NL-SH model gives $g_{\sigma K}^{\text{QM}} = 3.48$. The associated RMF K^- nuclear *scalar* potential, in the static

approximation, is given by:

$$V_{\text{RMF-scalar}}^{K^-} = -\frac{g_{\sigma K}^{\text{QM}} g_{\sigma N}^{\text{NL-SH}} \rho_0^s}{2 m_\sigma^2} = -66.3 \text{ MeV}, \quad (10)$$

using the values $m_\sigma = 526.1$ MeV from NL-SH and $\rho_0^s \approx 0.9\rho_0$, where ρ_0^s is the scalar density. Our choice of $g_{\sigma K}$ is conceptually different, fitting $g_{\sigma K}$ to several selected values of \bar{K} separation energy $B_{\bar{K}}$ in nuclear systems with a single \bar{K} meson. These fitted values, all of which were considerably lower than the QM value, are specified in the next section. Thus, our scalar potentials are viewed as a supplement to the minimal vector potentials discussed above to scan over \bar{K} nuclear binding energies in a given energy range, without imparting any microscopic meaning to these scalar potentials. We also tested the effect of adding another scalar-meson field that couples exclusively to strangeness, “hidden strangeness” σ^* meson with mass $m_{\sigma^*} = 980$ MeV, and coupling constant $g_{\sigma^* K} = 2.65$ determined from $f_0(980) \rightarrow K^+ K^-$ decay [12].

III. RESULTS AND DISCUSSION

A. Saturation of \bar{K} binding energies and hadronic densities

Following the observation made in Ref. [16] that \bar{K} binding energies, as well as nuclear and \bar{K} densities, saturate on increasing the number κ of \bar{K} mesons, we have explored how robust this saturation is. In particular we studied, for several selected nuclei across the periodic table, the role of various components of the \bar{K} -nucleus interaction in establishing saturation and the sensitivity to the choice of the RMF model. Representative examples are shown in Figs. 1 and 2.

Figure 1 presents the $1s$ K^- separation energy B_{K^-} in multi- K^- nuclei $^{16}\text{O} + \kappa K^-$ as a function of the number κ of K^- mesons, using the NL-SH RMF parametrization, for several mean-field compositions of the K^- self-energy Eq. (5) with K^- vector-meson couplings given by Eq. (8). The upper group of curves is based on a value of $g_{\sigma K} = 2.433$ ensuring $B_{K^-} = 100$ MeV for $\kappa = 1$. The ϕ, ρ, σ^* meson fields do not practically contribute in this case, whereas the Coulomb field adds a few MeV attraction and $\text{Im}V_{\text{opt}}$ adds a few MeV repulsion. For $\kappa > 1$, the various curves of the upper group diverge from each other: with respect to a “minimal” $\sigma+\omega$ model (open circles), the main contributors are the repulsive

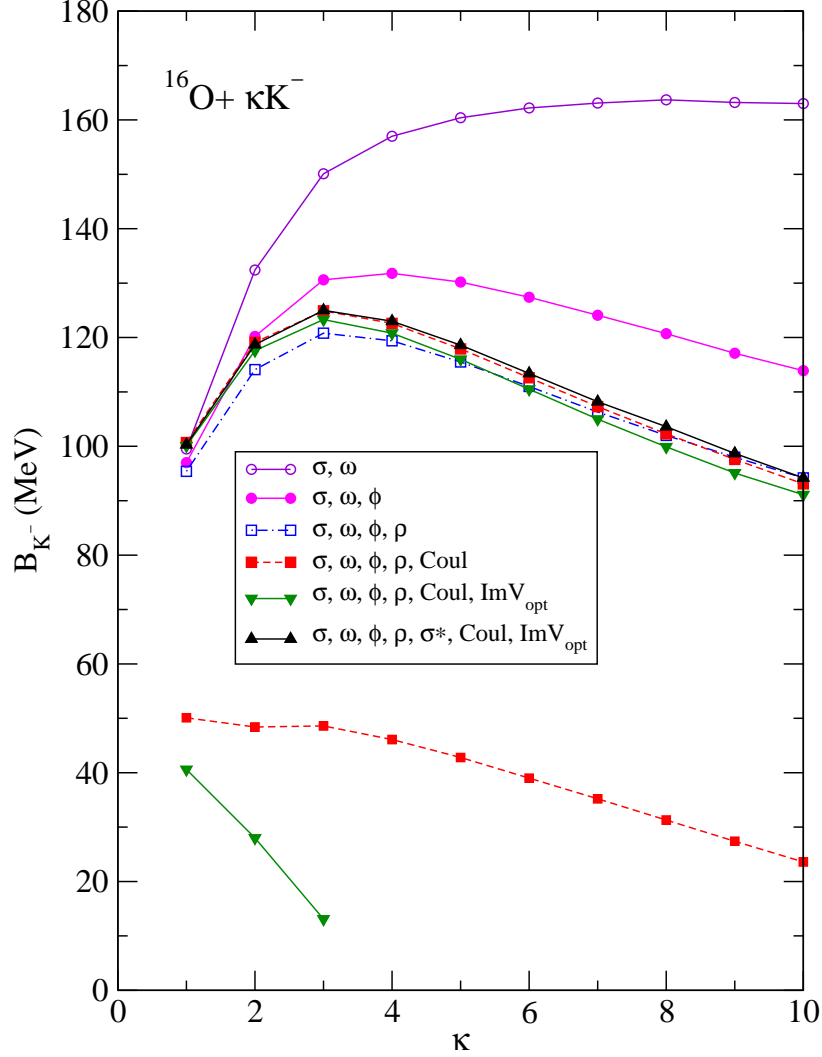


FIG. 1: $1s$ K^- separation energy B_{K^-} in $^{16}\text{O} + \kappa K^-$ as a function of the number κ of antikaons in several calculations detailed in the text, as listed in the inset, using the NL-SH RMF nuclear model with $g_{\sigma K} = 2.433$ for the upper group of curves and $g_{\sigma K} = 1.703$ for the lower group.

ϕ and ρ vector mesons, as judged by the curves marked by solid circles and open squares, respectively. Given their contributions, which get larger with κ , the inclusion of the Coulomb field, the σ^* meson field and $\text{Im}V_{\text{opt}}$ makes a small difference. However, the K^- absorptivity $\text{Im}V_{\text{opt}}$ makes a big difference for the lower group of curves consisting of only two choices, both with $g_{\sigma K} = 1.703$ fitted to $B_{K^-} \approx 40 - 50$ MeV for $\kappa = 1$. The energy dependence of $\text{Im}V_{\text{opt}}$ magnifies its effect for relatively low values of B_{K^-} in the region $B_{K^-} \leq 100$ MeV, adding significant repulsion the lesser the value of B_{K^-} is. This added repulsion (lowest curve in Fig. 1) leads to a rapid fall-off of B_{K^-} , terminating the binding at $\kappa = 3$, because

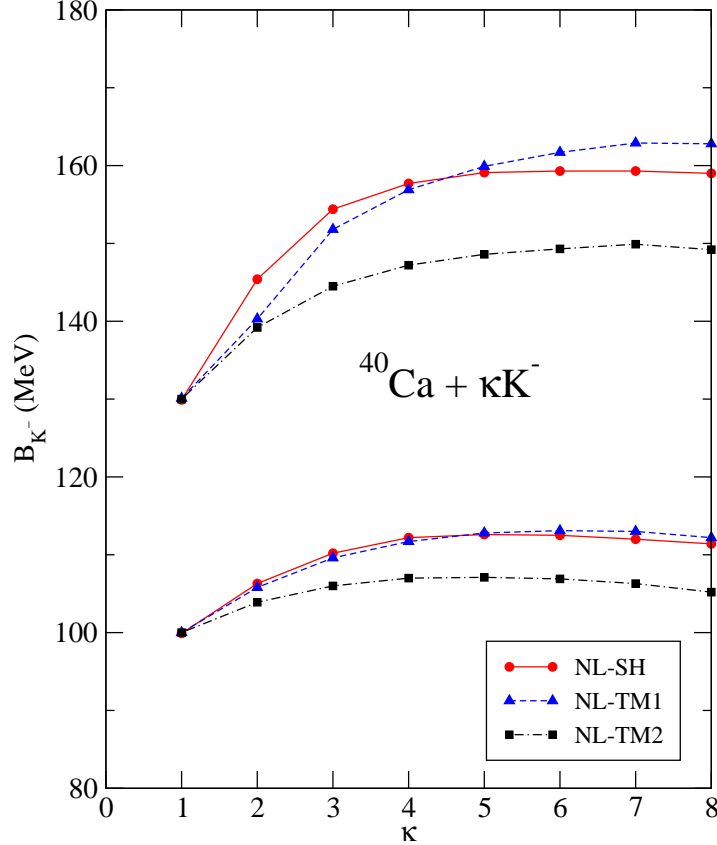


FIG. 2: $1s$ K^- separation energy B_{K^-} in $^{40}\text{Ca} + \kappa K^-$, as a function of the number κ of K^- mesons, calculated in the NL-SH (circles, solid lines), NL-TM1 (triangles, dashed lines), and NL-TM2 (squares, dot-dashed lines) RMF models. The lower (upper) group of curves was constrained to produce $B_{K^-} = 100$ (130) MeV for $\kappa = 1$.

the system $^{16}\text{O} + 4K^-$ is found to be unbound for this particular choice of $\kappa = 1$ parameters. The lesson from Fig. 1 is that saturation of the K^- binding energy in nuclear systems with κ K^- mesons is a robust phenomenon, which remains valid regardless of the type of meson fields mediating the strong interaction among antikaons and nucleons, provided a *minimal* isoscalar vector-meson field (ω) is included. For a sufficiently large number κ of K^- mesons, the combined repulsive K^-K^- interaction generated by the vector meson fields ω , ϕ , ρ wins over the attractive interaction generated by the isoscalar scalar-meson fields (dominated by σ). The effect of adding the σ^* scalar field is found to be insignificant. These conclusions hold also for a Lagrangian in which scalar fields are introduced differently than in Eq. (1), resulting in a correspondingly different definition of effective masses, $m_K^* = m_K - g_{\sigma K}\sigma_0 - g_{\sigma^* K}\sigma_0^*$ [29], than in Eq. (6).

Figure 2 shows the $1s$ K^- separation energy B_{K^-} in multi- K^- nuclei $^{40}\text{Ca} + \kappa K^-$ as a function of the number κ of K^- mesons, calculated in the NL-SH, NL-TM1, and NL-TM2 RMF models for two choices of $g_{\sigma K}$ designed, within each model, to produce $B_{K^-} = 100$ and 130 MeV for $\kappa = 1$. The values of $g_{\sigma K}$ for NL-SH were 1.703 and 2.993, respectively. The difference between the various curves, for a given starting value of B_{K^-} , originates from the specific balance in each one of these RMF models between the vector fields and the scalar field. The figure illustrates that the saturation of the \bar{K} binding energy in nuclear systems with several antikaons is not limited to a particular choice of RMF parametrization but is a general feature independent of the applied RMF model. Without loss of generality, we therefore specialize in the subsequent discussion to a specific RMF model, namely NL-SH.

The dependence of the nuclear density $\rho_N(r)$ and the K^- density $\rho_{K^-}(r)$ on the number κ of K^- mesons in multi- K^- nuclei $^{40}\text{Ca} + \kappa K^-$ is shown in Fig. 3. The coupling constant $g_{\sigma K} = 1.703$ was chosen such that the single- K^- configuration was bound by 100 MeV, the same as for the NL-SH lower curve in Fig. 2. The density distribution ρ_N for ^{40}Ca is also shown, for comparison, by the dotted curve in the upper panel. It is clear from this figure that the central nuclear density ρ_N saturates for $\kappa = 8$ at a value about twice larger than that for ρ_N in ^{40}Ca . In the lower panel, it is seen that the gradual increase of ρ_{K^-} with κ slows down with increasing κ .

The saturation of the nuclear density in multi- \bar{K} nuclei manifests itself also in the behavior of the \bar{K} effective mass in the nuclear medium, Eq. (6), as a function of the number κ of antikaons. This is illustrated for $^{208}\text{Pb} + \kappa K^-$ in Fig. 4. Note that the calculated effective mass distribution $m_{K^-}^*(r)$ remains almost independent of the number of K^- mesons over a large volume of the nucleus, for $r \geq 3-4$ fm, reflecting a similar κ independence of the scalar σ field through the underlying nuclear density. In fact, the σ field in this region is almost unaffected by the presence of K^- mesons, as demonstrated by the dashed curve which uses the “static” ^{208}Pb σ field from a purely nuclear RMF calculation. It is only within a relatively small region near the nuclear center, typically $r \leq 2-3$ fm, that the variation of $m_{K^-}^*(r)$ with κ gets to be more pronounced. However, $m_{K^-}^*(r = 0)$ quickly saturates, already for $\kappa \approx 8$. The figure demonstrates clearly that the concept of “nuclear matter” is far from being realized, even for a nucleus as large as ^{208}Pb and that conclusions made on \bar{K} binding and kaon condensation in finite nuclei, using nuclear-matter arguments, should be taken with a grain of salt.

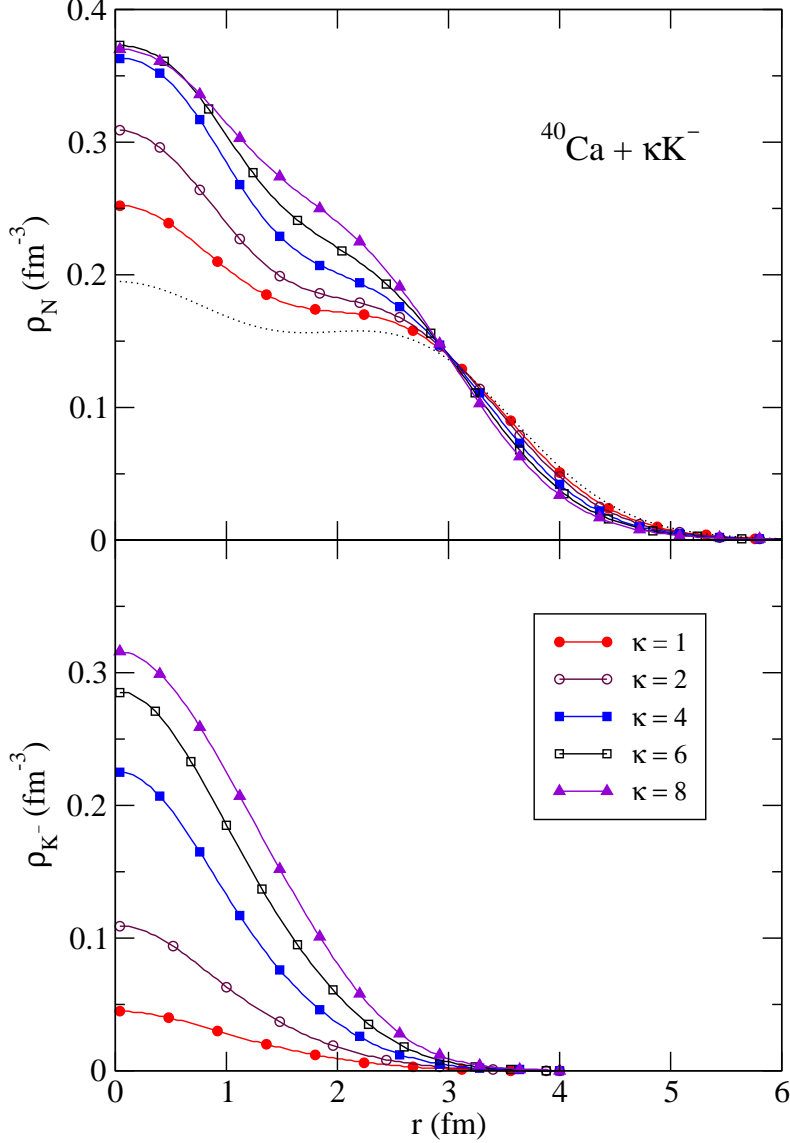


FIG. 3: Nuclear density ρ_N (top panel) and $1s$ K^- density ρ_{K^-} (bottom panel) in $^{40}\text{Ca} + \kappa K^-$, calculated in the NL-SH RMF model, with $g_{\sigma K} = 1.703$ chosen to yield $B_{K^-} = 100$ MeV in $^{40}\text{Ca} + 1K^-$. The dotted curve stands for the ^{40}Ca density in the absence of K^- mesons.

B. Exotic \bar{K} nuclear configurations

Because in the underlying $\bar{K}N$ dynamics the $I = 0$ interaction is considerably more attractive than the $I = 1$ interaction, we have looked for ways to maximize the role of the $\bar{K}N$ $I = 0$ channel in multi- \bar{K} nuclei. For a nuclear core with $N = Z$, no matter which charge states are assigned to the \bar{K} mesons, the average $\bar{K}N$ interaction is given by a $(2I + 1)$ -average which disfavors the $I = 0$ channel. This disadvantage is partly

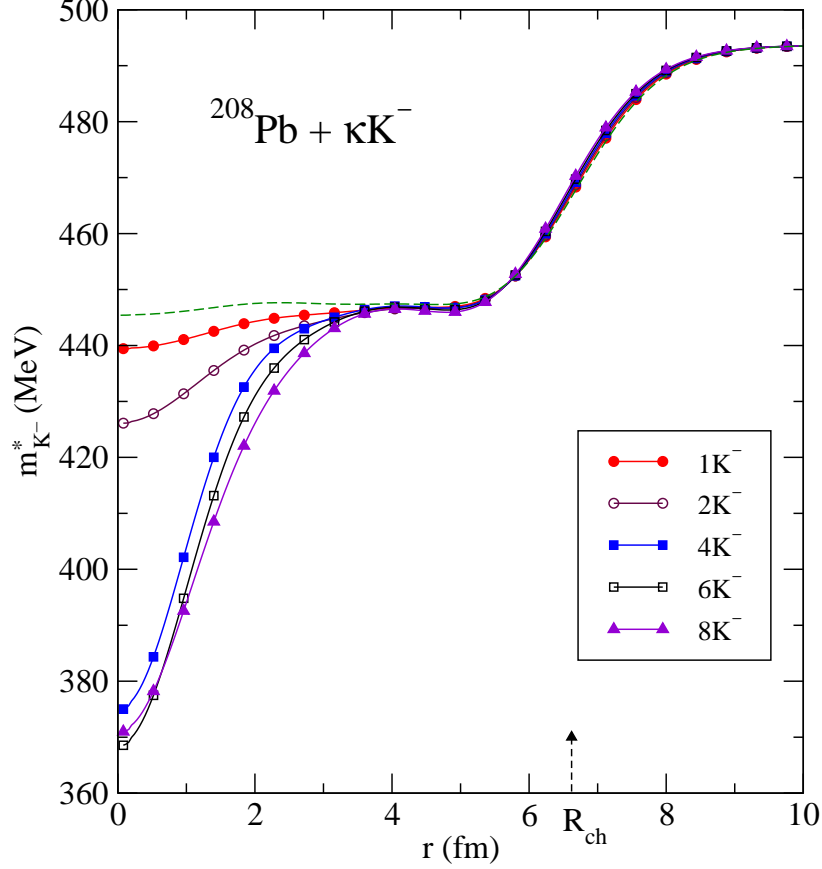


FIG. 4: $1s$ K^- effective mass $m_{K^-}^*$ in multi- K^- nuclei $^{208}\text{Pb} + \kappa K^-$, calculated in the NL-SH model with $g_{\sigma K} = 2.433$ chosen to yield $B_{K^-} = 100$ MeV in $^{208}\text{Pb} + 1K^-$. The dashed curve stands for the “static” case where the ^{208}Pb σ field in a purely nuclear RMF calculation was used in Eq. (6) for $m_{K^-}^*$. The dashed arrow indicates the charge half-density radius R_{ch} in ^{208}Pb .

removed by considering $n\bar{K}^0$ (or pK^-) multi- \bar{K} nuclei, where both isospin channels assume equal weight, so that the stronger $I = 0$ component may provide sufficient attraction to overcome the insufficient attraction in purely neutron matter. We therefore studied exotic configurations consisting solely of \bar{K}^0 mesons bound to neutrons. Our calculations confirmed that \bar{K} mesons can bind together systems of nucleons that otherwise are unbound.

In Fig. 5, we compare the separation energies $B_{\bar{K}}$ in $16n + \kappa\bar{K}^0$ and in $8n + \kappa\bar{K}^0$ exotic multi- \bar{K} configurations with $B_{\bar{K}}$ in $^{16}\text{O} + \kappa K^-$ multi- \bar{K} nuclei, most of which were calculated in the NL-SH RMF model with the “canonical” $g_{\nu K}$ coupling constants of Eq. (8) and $g_{\sigma K} = 2.433$ chosen to yield $B_{K^-} = 100$ MeV in $^{16}\text{O} + 1K^-$ as in Fig. 1, and for $\text{Im}V_{\text{opt}} = 0$. For each sequence of multi- \bar{K} nuclei, $B_{\bar{K}}$ increases as a function of κ to a maximum value

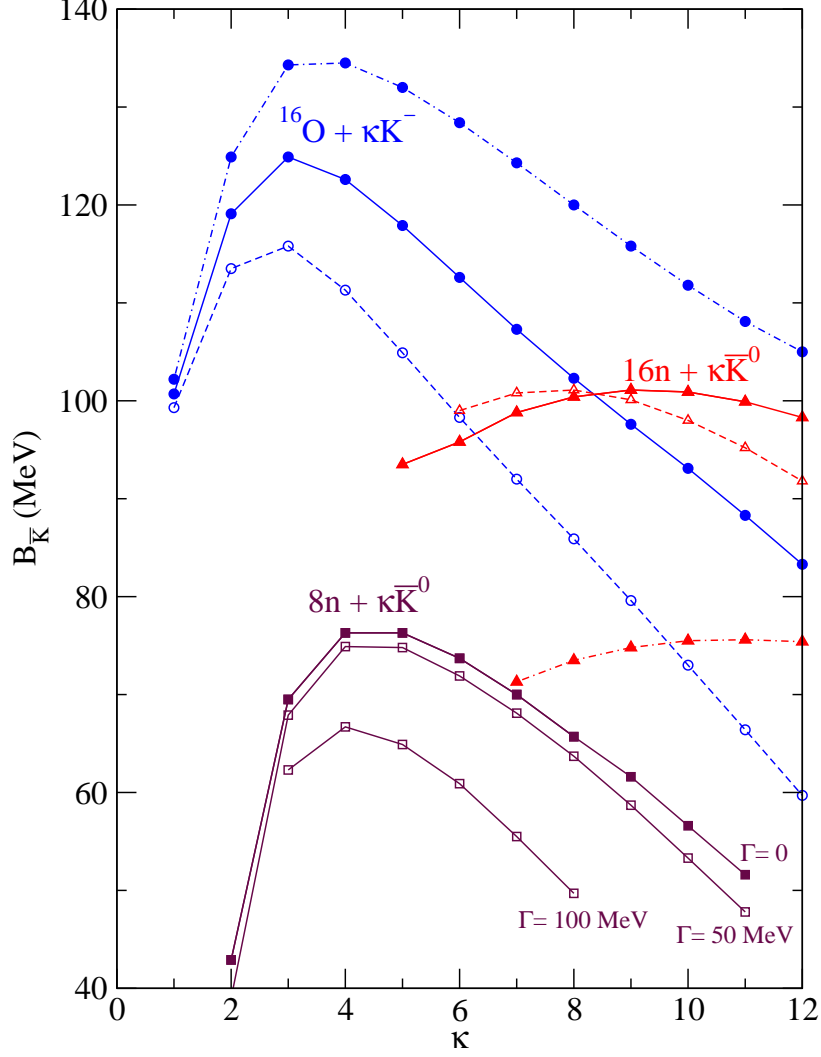


FIG. 5: $1s$ \bar{K} separation energy $B_{\bar{K}}$ in $^{16}\text{O} + \kappa \bar{K}^-$, $16n + \kappa \bar{K}^0$, and $8n + \kappa \bar{K}^0$, as a function of κ , calculated in the NL-SH RMF model, with $g_{\rho K} = 0$ (dot-dashed curves), $g_{\rho K}^{\text{SU}(3)} = 3.02$ (solid curves) and $g_{\rho K} = g_{\rho N} = 4.38$ (dashed curves). $\text{Im}V_{\text{opt}} = 0$ is assumed everywhere except for the two lowest solid curves (open squares) in $8n + \kappa \bar{K}^0$ where $\text{Im}V_{\text{opt}} \neq 0$, such that the value of width $\Gamma_{\bar{K}^0}$ is held fixed at 50 and 100 MeV, respectively, see text.

and then starts to decrease. Whereas the sequence consisting of 8 neutrons plus \bar{K}^0 mesons starts with $\kappa = 1$ (not shown in the figure), a larger number of neutrons generally requires a threshold value for κ as shown for the sequences consisting of 16 neutrons plus \bar{K}^0 mesons. Exceptions to the use of the canonical g_{vK} set of Eq. (8), or to $\text{Im}V_{\text{opt}} = 0$, are as follows:

- $g_{\rho K}^{\text{SU}(3)} = 3.02$ was used everywhere except for $g_{\rho K} = 0$ in the dot-dashed curves and except for $g_{\rho K} = g_{\rho N} = 4.38$ (universal isospin coupling) in the dashed curves to study

the role of the ρ meson in “nonexotic” multi- \bar{K} nuclei ($^{16}\text{O}+\kappa K^-$) and in “exotic” ones ($16n+\kappa\bar{K}^0$). In $^{16}\text{O}+\kappa K^-$, the values of B_{K^-} for a given value of $\kappa > 1$ decrease as $g_{\rho K}$ is increased, as expected from the *repulsive* K^-K^- isovector interaction. In contrast, the larger the value of $g_{\rho K}$ is, the larger is the value of $B_{\bar{K}^0}$ expected in $16n+\kappa\bar{K}^0$, because it is the ρ isovector interaction that distinguishes the more attractive $I = 0$ component of the \bar{K}^0n interaction from the less attractive $I = 1$ component. Indeed, this holds for $\kappa \leq 8$ in the figure. However, for $\kappa > 8$, the contribution of the repulsive $\bar{K}^0\bar{K}^0$ isovector interaction becomes substantial for the values of $g_{\rho K} \neq 0$ used here; the $B_{\bar{K}^0}$ dashed curve for the universal ρ coupling heads down, crossing the $B_{\bar{K}^0}$ solid curve corresponding to SU(3) ρ coupling. All in all, substantial binding in $16n+\kappa\bar{K}^0$ multi- \bar{K} nuclei is reached for these values of $g_{\rho K} \neq 0$.

- The effect of $\text{Im}V_{\text{opt}}$ on $B_{\bar{K}}$ is relatively unimportant for $B_{\bar{K}} \geq 100$ MeV, where the dominant $\bar{K}N \rightarrow \pi\Sigma$ decay channel is closed. The inclusion of $\text{Im}V_{\text{opt}}$ is found then to induce repulsion of less than 5 MeV. However, in $8n+\kappa\bar{K}^0$ multi- \bar{K} nuclei, where $B_{\bar{K}^0} \leq 80$ MeV, the effect of $\text{Im}V_{\text{opt}}$ becomes significant. An estimate of this effect is given by comparing the $B_{\bar{K}^0}$ curve for $\Gamma = 0$ (solid squares) with the $B_{\bar{K}^0}$ curves using $\text{Im}V_{\text{opt}} \neq 0$ (open squares) such that the value of $\Gamma_{\bar{K}^0}$ is *held fixed* at 50 and 100 MeV. As expected, the larger input widths induce a stronger repulsion that lowers the calculated $B_{\bar{K}^0}$ values. Yet considerably lower values of $B_{\bar{K}^0}$ are obtained once the \bar{K}^0 widths are included self-consistently in these dynamical calculations.

The nucleon-density distribution $\rho_N(r)$ and the \bar{K} -density distribution $\rho_{\bar{K}}(r)$ are shown in Fig. 6 for $^{16}\text{O}+8K^-$, $16n+8\bar{K}^0$, and $8n+8\bar{K}^0$. We note that ρ_N and $\rho_{\bar{K}}$ are normalized to the number of nucleons and number of antikaons, respectively. The \bar{K} couplings were chosen such that the $1K^-$ configuration in ^{16}O is bound by 100 MeV, as in Fig. 5. For comparison, we also present the density distribution ρ_N for ^{16}O without \bar{K} mesons. Owing to the substantial \bar{K} density $\rho_{\bar{K}}$ in the nuclear center, the central nuclear density $\rho_N(0)$ in all three systems with 8 \bar{K} mesons is about 2-3 times larger than the central nuclear density ρ_0 in ^{16}O for $\kappa = 0$. The situation is particularly pronounced in $8n+8\bar{K}^0$, with the same central density $\rho_N(0)$ as in the systems with 16 nucleons + $8\bar{K}$. Furthermore, the $8n+8\bar{K}^0$ system is compressed substantially in comparison with the other multi- \bar{K} systems, judging by the radial extension of ρ_N and $\rho_{\bar{K}}$ in both panels of Fig. 6. The relatively high value $\rho_{\bar{K}}(0) \sim 5\rho_0$

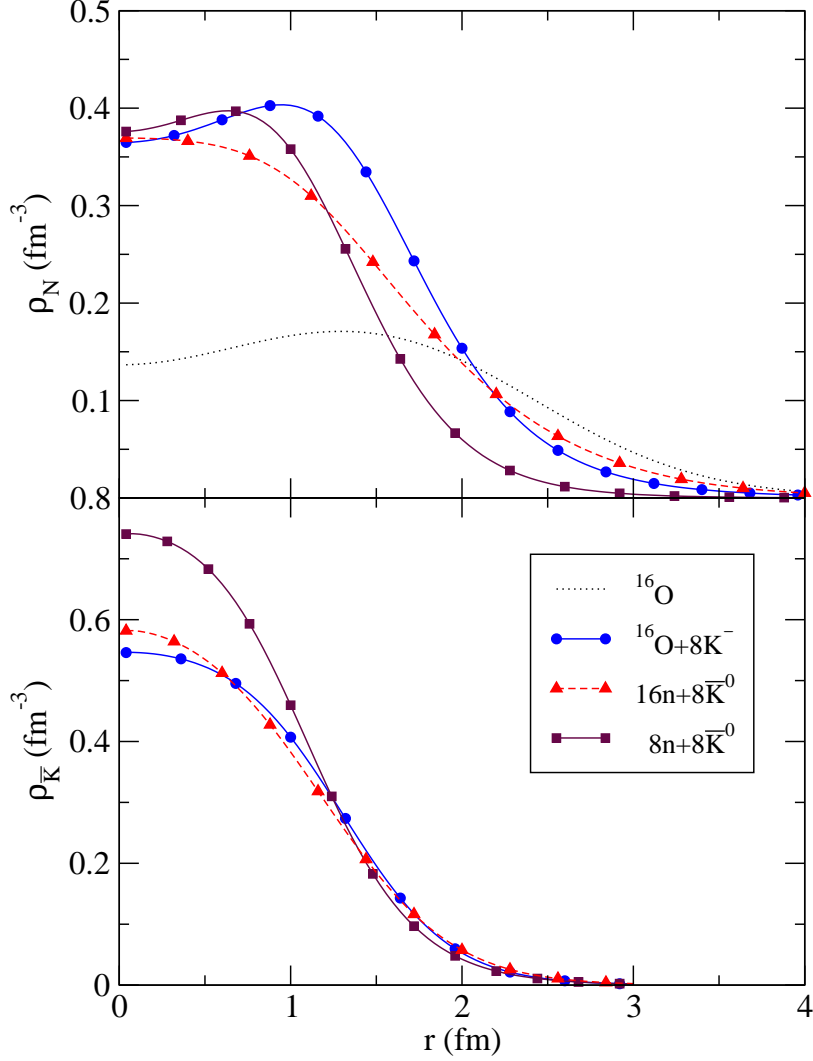


FIG. 6: Nuclear density ρ_N (top panel) and $1s$ \bar{K} density $\rho_{\bar{K}}$ (bottom panel) in $^{16}\text{O}+8K^-$, $16n+8\bar{K}^0$ and $8n+8\bar{K}^0$, calculated in the NL-SH RMF model, with the “canonical” g_{vK} coupling constants of Eq. (8) and with $g_{\sigma K} = 2.433$ to yield $B_{K^-} = 100$ MeV in $^{16}\text{O}+1K^-$ as in Fig. 5. The dotted curve stands for the ^{16}O density in the absence of \bar{K} mesons.

for this system does not introduce complications due to possible overlap between antikaons, because the mean-square radius of K^- is less than half of the corresponding quantity for the proton [30, 31].

Given the compressed nuclear densities plotted in Fig. 6, we show in Fig. 7 the calculated neutron single-particle energy levels in ^{16}O , in $^{16}\text{O}+\kappa K^-$ and in $8n+\kappa\bar{K}^0$ multi- \bar{K} nuclei for $\kappa = 4, 8$. The \bar{K} couplings are the same as in Figs. 5 and 6, again chosen to ensure $B_{K^-} = 100$ MeV in $^{16}\text{O}+1K^-$. The $1s_{1/2}$ and $1p_{3/2}$ levels undergo increasingly attractive

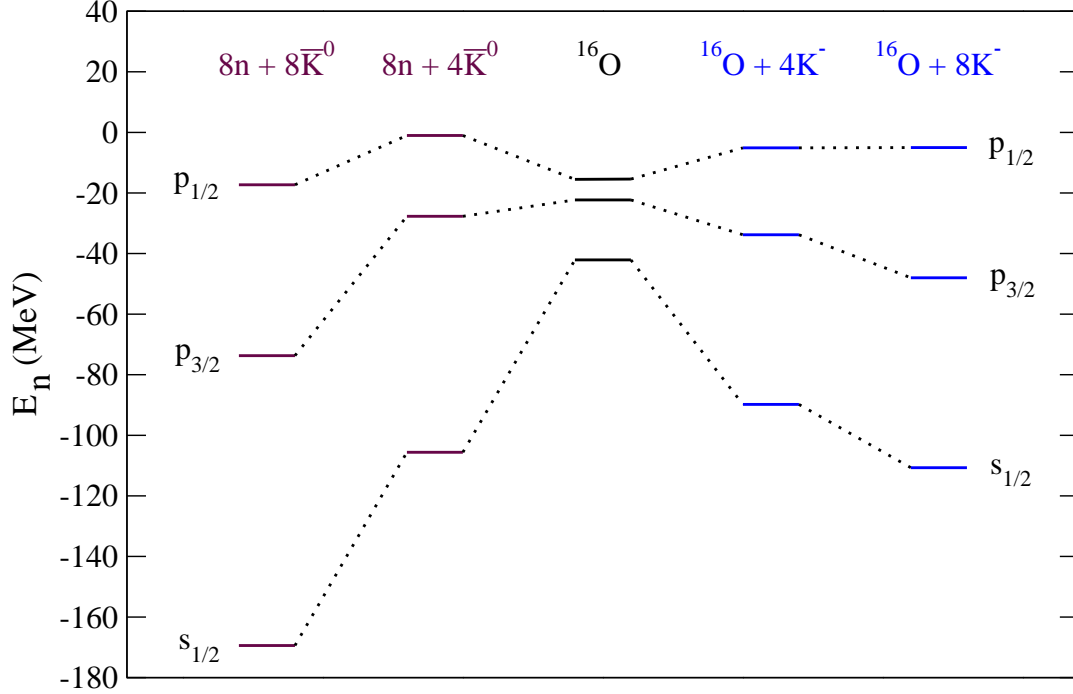


FIG. 7: Neutron single-particle spectra in ^{16}O (center) $^{16}\text{O}+4(8)\bar{K}^-$ (right) and $8n+4(8)\bar{K}^0$ (left), calculated in the NL-SH RMF model with $g_{\sigma K} = 2.433$ chosen to yield $B_{K^-} = 100$ MeV in $^{16}\text{O}+1\bar{K}^-$.

shifts on varying κ in these multi- \bar{K} systems. Particularly strong is the downward shift of the $1s_{1/2}$ level, by about 70 MeV in $^{16}\text{O}+8\bar{K}^-$ and by about 130 MeV in $8n+8\bar{K}^0$. In contrast, the $1p_{1/2}$ neutron level is pushed up by about 10 MeV in the $^{16}\text{O}+\kappa\bar{K}^-$ systems as a result of a gradually increasing spin-orbit splitting which reaches 43 MeV for $\kappa = 8$ (recall that it is 7 MeV for $\kappa = 0$ using NL-SH). The $1p_{1/2}$ neutron level is weakly bound in the exotic $8n+\kappa\bar{K}^0$ systems for $1 < \kappa < 6$, getting more bound with κ as shown in the figure for these systems. The $1p$ spin-orbit splitting becomes as large as 56 MeV in the exotic $8n+8\bar{K}^0$ system which exhibits the largest single-particle level splittings in this figure. Here the $1p_{1/2}$ neutron level, too, undergoes attraction.

It is worth mentioning that exotic multi- \bar{K}^0 configurations that contain no protons lie high in the continuum of “nonexotic” multi- \bar{K} nuclei that are based on nuclear cores with protons and neutrons. Figure 8 shows the calculated *total* binding energy $B[A, Z, \kappa\bar{K}]$, Eq. (7), assuming for simplicity $g_{\rho K} = 0$, for three sequences of multi- \bar{K} nuclei. To illustrate the relationship between “exotic” and “nonexotic” configurations, we take the $16n+8\bar{K}^0$ configuration, specifically in its lowest isospin $I = 4$ state, and replace successively \bar{K}^0+n

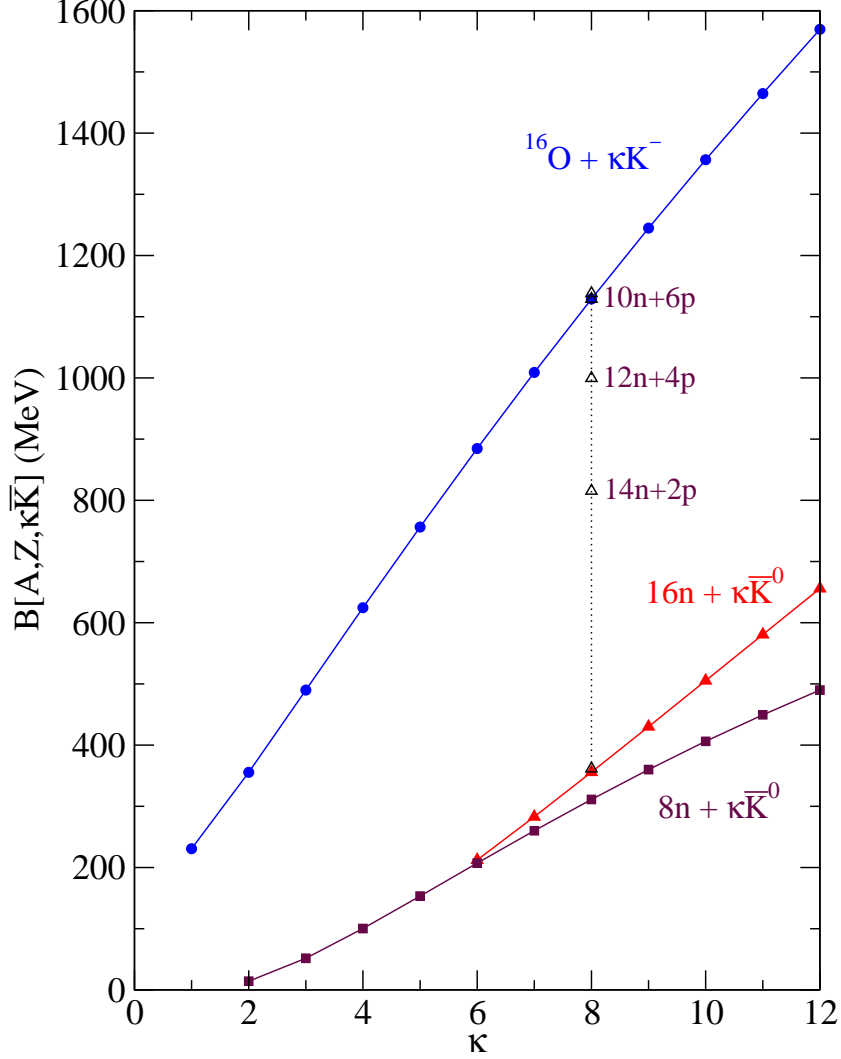


FIG. 8: Total binding energy $B[A, Z, \kappa\bar{K}]$ of $^{16}\text{O} + \kappa\bar{K}^-$ (circles), $16n + \kappa\bar{K}^0$ (solid triangles) and $8n + \kappa\bar{K}^0$ (squares) multi- \bar{K} systems, as a function of κ , calculated in the NL-SH RMF model with $g_{\sigma K} = 2.433$ chosen to yield $B_{K^-} = 100$ MeV in $^{16}\text{O} + 1\bar{K}^-$, and with $g_{\rho K} = 0$. For $\kappa = 8$, total binding energy values for configurations that are intermediate between $^{16}\text{O} + 8\bar{K}^-$ and $16n + 8\bar{K}^0$ are shown in open triangles along the dashed line.

pairs by $K^- + p$ pairs until $^{16}\text{O} + 8\bar{K}^-$ is reached. This is demonstrated by the empty triangles along the vertical dotted line that connects the initial and final configurations. Both initial and final configurations have identical quantum numbers $B = 8$, $Q = 0$, $I = 4$, so they are commensurate. Therefore, although \bar{K} mesons are capable of stabilizing purely neutron configurations, these exotic configurations do not compete energetically with multi- \bar{K} nuclei based on nuclear cores along the nuclear valley of stability.

IV. SUMMARY

In the main part of this work, we studied several dynamical aspects of multi- \bar{K} nuclear states within RMF methodology. In particular, we discussed in detail the saturation pattern of \bar{K} separation energies and nuclear densities on increasing the number of antikaons embedded in the nuclear medium. Saturation was demonstrated to be a robust feature of multi- \bar{K} nuclei. The saturated values of $B_{\bar{K}}$, for “natural” values of meson-field coupling constants were found generally to be below 200 MeV, considerably short of the threshold value ≈ 320 MeV needed for the onset of kaon condensation under laboratory conditions. We conclude, consistently with our earlier conjecture [16], that \bar{K} mesons do not provide the physical “strangeness” degrees of freedom for self-bound strange dense matter.

We first explored contributions of specific meson mean fields to the \bar{K} separation energy $B_{\bar{K}}$. Saturation of $B_{\bar{K}}$ emerged for any boson-field composition that includes the dominant vector ω -meson field, using the “minimal” SU(3) value suggested by the leading-order Tomozawa-Weinberg term of the meson-baryon effective Lagrangian. Moreover, the contribution of each one of the vector ϕ -meson and ρ -meson fields was found to be substantially repulsive for systems with a large number of antikaons, reducing the \bar{K} separation energy as well as lowering the threshold value of number of antikaons required for saturation to occur. In contrast, the Coulomb interaction and the addition of a hidden-strangeness scalar σ^* -meson field have little effect on the binding energy balance and on the pattern of saturation.

We also verified that the saturation behavior of $B_{\bar{K}}$ is qualitatively independent of the RMF model applied to the nucleonic sector. The onset of saturation was found to depend on the atomic number. Generally, the heavier the nucleus is, the more antikaons it takes to saturate their separation energies.

The saturation phenomenon found for the \bar{K} separation energy is also reflected in the nucleon and antikaon density distributions, with the assertions made above remaining valid. The saturation of the nuclear density in multi- \bar{K} nuclei manifests itself in the behavior of the \bar{K} effective mass distribution in the nuclear medium. We stress that in the case of antikaons the concept of nuclear matter is far from being realized even in such a heavy nucleus as ^{208}Pb . Specifically, the reduction of $m_{\bar{K}}^*(r)$ on adding \bar{K} mesons is pronounced only within a small region around the nuclear center.

In the second part of this work, we studied exotic configurations consisting exclusively of neutrons and \bar{K}^0 mesons. We demonstrated that a finite number of neutrons can be made self-bound by adding few \bar{K}^0 mesons, with the resulting nuclear configurations more tightly bound than ordinary nuclei. Saturation of $B_{\bar{K}^0}$ was found for these exotic configurations too. Yet, these exotic configurations consisting exclusively of neutrons and \bar{K}^0 mesons lie high in the continuum of the less exotic multi- \bar{K} configurations based on nuclear cores along the nuclear valley of stability.

In conclusion, over a wide range of variations our calculations do not indicate any precursor phenomena to kaon condensation in self-bound strange nuclear systems.

Acknowledgments

This work was supported in part by the GA AVCR grant IAA100480617 and by the Israel Science Foundation grant 757/05.

-
- [1] D.B. Kaplan, A.E. Nelson, Phys. Lett. B **175**, 57 (1986); *ibid* **B179**, 409 (1986).
 - [2] A.E. Nelson, D.B. Kaplan, Phys. Lett. B **192**, 193 (1987).
 - [3] E. Friedman, A. Gal, Phys. Rep. **452**, 89 (2007); and earlier references cited therein.
 - [4] W. Scheinast *et al.*, Phys. Rev. Lett. **96**, 072301 (2006); and earlier references to nucleus-nucleus experiments cited therein.
 - [5] C.B. Dover, P.J. Moffa, Phys. Rev. C **16**, 1087 (1977).
 - [6] C.-H. Lee, Phys. Rep. **275**, 255 (1996).
 - [7] M. Prakash, I. Bombaci, M. Prakash, P.J. Ellis, J.M. Lattimer, R. Knorren, Phys. Rep. **280**, 1 (1997).
 - [8] H. Heiselberg, M. Hjorth-Jensen, Phys. Rep. **328**, 237 (2000).
 - [9] H. Heiselberg, V.R. Pandharipande, Annu. Rev. Nucl. Part. Sci. **50**, 481 (2000).
 - [10] N.K. Glendenning, Phys. Rep. **342**, 393 (2001).
 - [11] A. Ramos, J. Schaffner-Bielich, J. Wambach, Lect. Notes Phys. **578**, 175 (2001).
 - [12] J. Schaffner, I.N. Mishustin, Phys. Rev. C **53**, 1416 (1996).
 - [13] P.J. Ellis, R. Knorren, M. Prakash, Phys. Lett. B **349**, 11 (1995).

- [14] T. Yamazaki, A. Doté, Y. Akaishi, *Phys. Lett. B* **587**, 167 (2004).
- [15] J. Schaffner-Bielich, A. Gal, *Phys. Rev. C* **62**, 034311 (2000); and references cited therein.
- [16] D. Gazda, E. Friedman, A. Gal, J. Mareš, *Phys. Rev. C* **76**, 055204 (2007).
- [17] J. Mareš, E. Friedman, A. Gal, *Phys. Lett. B* **606**, 295 (2005).
- [18] J. Mareš, E. Friedman, A. Gal, *Nucl. Phys. A* **770**, 84 (2006).
- [19] W. Weise, *Proc. IX Int. Conf. Hypernuclear and Strange Particle Physics*, Eds. J. Pochodzalla and Th. Walcher (SIF and Springer-Verlag, Berlin Heidelberg, 2007) p. 243 [arXiv:nucl-th/0701035]; W. Weise, R. Härtle, *Nucl. Phys. A* **804**, 173 (2008).
- [20] N.V. Shevchenko, A. Gal, J. Mareš, *Phys. Rev. Lett.* **98**, 082301 (2007).
- [21] N.V. Shevchenko, A. Gal, J. Mareš, J. Révai, *Phys. Rev. C* **76**, 044004 (2007).
- [22] Y. Ikeda, T. Sato, *Phys. Rev. C* **76**, 035203 (2007).
- [23] E. Friedman, A. Gal, J. Mareš, A. Cieplý, *Phys. Rev. C* **60**, 024314 (1999).
- [24] M.M. Sharma, M.A. Nagarajan, P. Ring, *Phys. Lett. B* **312**, 377 (1993).
- [25] Y. Sugahara, H. Toki, *Nucl. Phys. A* **579**, 557 (1994).
- [26] Th.A. Rijken, *Phys. Rev. C* **73**, 044007 (2006).
- [27] A. Martinez Torres, K.P. Khemchandani, E. Oset, submitted to *Eur. Phys. J. A*, arXiv:0712.1938 [nucl-th].
- [28] P. Finelli, N. Kaiser, D. Vretenar, W. Weise, *Nucl. Phys. A* **770**, 1 (2006).
- [29] N.K. Glendenning, J. Schaffner-Bielich, *Phys. Rev. Lett.* **81**, 4564 (1998).
- [30] S.R. Amendolia *et al.*, *Phys. Lett. B* **178**, 435 (1986).
- [31] G. Simon, C. Schmitt, F. Borkowski, V. Walther, *Nucl. Phys. A* **333**, 381 (1980).